Monthly Notices of the ROYAL ASTRONOMICAL SOCIETY

MNRAS **497,** 4311–4321 (2020) doi:10.1093/mnras/staa2202
Advance Access publication 2020 July 29

How unusual is the Milky Way's assembly history?

Tilly A. Evans ,★ Azadeh Fattahi , Alis J. Deason and Carlos S. Frenk
Institute for Computational Cosmology, Department of Physics, Durham University, South Road, Durham DH1 3LE, UK

Accepted 2020 July 22. Received 2020 July 13; in original form 2020 May 11

ABSTRACT

In the lambda cold dark matter (ΛCDM) model of structure formation galactic haloes build-up by accretion of mass and mergers of smaller haloes. The most recent massive merger event experienced by the Milky Way (MW) halo was the accretion of the Large Magellanic Cloud (LMC; which has a stellar mass of $\sim 10^9$ $M_\odot$). Recent analyses of galactic stellar data from the *Gaia* satellite have uncovered an earlier massive accretion event, the Gaia-Enceladus Sausage (GES), which merged with the MW around 10 Gyr ago. Here, we use the EAGLE cosmological hydrodynamics simulation to study properties of simulated MW-mass haloes constrained to have accretion histories similar to that of the MW, specifically the recent accretion of an 'LMC' galaxy and a 'GES' merger, with a quiescent period between the GES merger and the infall of the LMC (the 'LMC and GES' category). We find that ∼16 per cent of MW-mass haloes have an LMC; ∼5 per cent have a GES event and no further merger with an equally massive object since $z = 1$; and only 0.65 per cent belong to the LMC and GES category. The progenitors of the MWs in this last category are much less massive than average at early times but eventually catch up with the mean. The LMC and GES category of galaxies naturally end up in the 'blue cloud' in the colour–magnitude diagram at $z = 0$, tend to have a disc morphology and have a larger than average number of satellite galaxies.

Key words: Methods: numerical – Galaxy: evolution – Galaxy: formation.

1 INTRODUCTION

The Milky Way (MW) is sometimes regarded as a template for studies of the structure and evolution of $L^\star$ spiral galaxies. Yet, the more we find out about the MW, the more we recognize that it is anything but typical; in fact, several of its properties are distinctly atypical. For example, the MW hosts a very massive satellite, the Large Magellanic Cloud (LMC), which has approximately 10 per cent of the total MW halo mass (e.g. Benson et al. 2002; Penarrubia et al. 2016; Shao et al. 2018). Studies using large samples of observed local galaxies, combined with cosmological simulations, find that only ∼ 10 per cent of MW-mass galaxies host a satellite as massive as this (e.g. Boylan-Kolchin, Bullock & Kaplinghat 2011; Busha et al. 2011; Liu et al. 2011; Tollerud et al. 2011). Not only is the presence of a massive satellite rare, but the scale of the damage the LMC is inflicting on the Galaxy has recently began to be recognized. This includes perturbing the barycentre of the MW (Gomez et al. 2015), disturbing the Galactic disc (Laporte et al. 2018) and inducing a large-scale gravitational 'wake' in the stellar and dark matter haloes (Garavito-Camargo et al. 2019). Clearly the accretion of the LMC is a significant, transformative event in our Galaxy's history.

In addition to hosting the LMC, the MW has other peculiarities. Its central supermassive black hole has an abnormally small mass compared to other galaxies of similar stellar mass (e.g. Savorgnan et al. 2016); its satellite system has a strange planar alignment perpendicular to the MW disc (e.g. Lynden-Bell 1976; Libeskind et al. 2005; Metz, Kroupa & Libeskind 2008); the chemodynamical properties of the bulge suggest an uncommonly quiet merger history (Fragkoudi et al. 2020); and the Galactic stellar halo may be unusually low mass and metal poor (e.g. Bell et al. 2017; Harmsen et al. 2017, but see Conroy et al. 2019; Deason, Belokurov & Sanders 2019). Some of these seemingly atypical qualities could be explained by the paucity of mergers experienced by our Galaxy. For example, it is expected that our forthcoming merger with the LMC (in a couple of gigayears time) may return the MW back to 'normality' (Cautun et al. 2019). In view of all these peculiarities, a natural question to ask is how similar or different is the MW assembly history to that of other galaxies of similar mass?

A fundamental prediction of the lambda cold dark matter (ΛCDM) model is that MW-mass galaxies grow by accretion and mergers with smaller galaxies. Simulations show that large stellar haloes form as a result of these accretion events (Bullock & Johnston 2005; Abadi, Navarro & Steinmetz 2006; Font et al. 2006; Cooper et al. 2010). Dynamical time-scales in the stellar halo are long, so the phase-space distribution of halo stars can retain some memory of the past accretion events. Moreover, the chemistry of the debris of merger events reflects that of the progenitor galaxies: more massive dwarfs are more metal rich than lower mass dwarfs, and have distinct sequences in chemical abundance space (e.g. Tolstoy, Hill & Tosi 2009). Hence, by analysing the stellar phase-space and chemistry properties, it may be possible to identify different accretion events. The link between the chemodynamics of halo stars and the Galaxy's assembly history can be traced back to the early work by Eggen, Lynden-Bell & Sandage (1962). More recently, our view of the Galaxy has been transformed by the availability of 6D phase-space information for large numbers of halo stars provided by large astrometric, photometric, and spectroscopic surveys.

★ E-mail: tilly.evans@durham.ac.uk

The *Gaia* mission, in particular, is providing new detailed insights into the assembly history of the MW. The first and second data releases led to the discovery of an ancient merger event, discovered independently by two teams who called it 'Gaia Enceladus' (Helmi et al. 2018) and 'Gaia Sausage' (Belokurov et al. 2018), respectively; here we will refer to both jointly as the Gaia-Enceladus Sausage (GES).[1]

Helmi et al. (2018) analysed the kinematics, chemistry, and positions of stars in the MW's thick disc and stellar halo, and found that high-energy stars on retrograde orbits are also linked by their chemical compositions. They concluded that the inner halo is dominated by stars coming from a single object accreted around 8–11 Gyr ago. Belokurov et al. (2018) used kinematics and chemistry of stars from SDSS and *Gaia* DR1 to show that, at higher metallicity ([Fe/H]>1.7), the orbits of the halo stars are very radially biased (with velocity anisotropy, $\beta \sim 0.9$). These authors argue that the extreme radial orbits in the inner stellar halo cannot have been caused by steady accretion of low-mass dwarf galaxies, but instead must have come from a single merger event with a massive satellite some 8–11 Gyr ago. This proposal agrees with the idea of orbit radialization put forward by Amorisco (2017). The connection between highly radial orbits and massive merger events has been confirmed with cosmological simulations (e.g. Fattahi et al. 2019; Mackereth et al. 2019).

In addition to halo stars, globular clusters can be used to identify accreted dwarf galaxies since, by virtue of their high stellar mass density, they are able to survive tidal disruption long after the dwarf galaxy, that brought them into the MW, has been destroyed (e.g. Kruijssen & Portegies Zwart 2009; Penarrubia, Walker & Gilmore 2009). Recent work using *Gaia* DR2 shows that the Galactic globular cluster population also points to a GES merger event (Myeong et al. 2018; Pfeffer et al. 2020). In particular, Myeong et al. (2018) show that at least eight Galactic globular clusters are likely to be associated with the GES. However, in addition to the GES, the globular cluster population has possibly revealed two additional merger events: Sequoia and Kraken (Myeong et al. 2019; Kruijssen et al. 2020). Sequoia is thought to have merged with the MW around the same time as the GES, but the progenitor had a much lower mass (Myeong et al. 2019). Kraken is thought to be much older (accretion at $z > 2$), but may have an even higher mass ratio relative to the MW than the GES merger (Pfeffer et al. 2020). The existence of this latter event is still under debate, and it may be more difficult to identify in the halo stars as its stellar debris likely occupies the inner few kiloparsecs of the Galaxy.

In view of the recent advances in our knowledge of the assembly history of the MW, the aim of this paper is to characterize MW-like galaxies in cosmological simulations that have similar past accretion events to our own galaxy. Specifically, we use the cosmological hydrodynamics EAGLE simulation (Crain et al. 2015; Schaye et al. 2015) to identify MW-mass systems that underwent mergers analogous to *both* the LMC and GES events. Previous studies have considered MW-like galaxies with either an LMC *or* a GES event (e.g. Bignone, Helmi & Tissera 2019; Cautun et al. 2019; Elias et al. 2020), but not both as seems appropriate for the actual MW. The 'classical' view of the LMC (e.g. Cautun et al. 2019) allows for a variety of previous mergers but does not include the paucity of massive merger events experienced by the MW between the recent infall of the LMC and the ancient merger of the GES. This paper aims to explore differences among galaxies that experience late (LMC), early (GES) merger events, or both. In particular, we aim to establish how unusual it is for an MW-mass galaxy to have both these events and a dearth of massive mergers in between.

The paper is arranged as follows. In Section 2, we describe the simulations used for our analysis and our sample selection. In Section 3, we present our results; we discuss and summarize our conclusions in Section 4.

[1]Note, however, that it is still debated whether or not these two discoveries are describing exactly the same event (e.g. Elias et al. 2020; Evans 2020).

2 SIMULATIONS

We now give a brief overview of the EAGLE simulations. We also describe the selection criteria for our MW-mass galaxies, and the reasoning behind each choice.

2.1 EAGLE

We aim to identify MW analogues in the EAGLE simulation (Crain et al. 2015; Schaye et al. 2015; McAlpine et al. 2016), which have either an LMC-mass satellite, an ancient merger similar to the GES, or both an LMC and a GES event. The EAGLE project is a suite of cosmological hydrodynamical simulations that follow the formation and evolution of galaxies, tracking the gas, stars, and dark matter throughout cosmic history. The simulations use a modified version of the Tree-PM SPH code P-GADGET3, which is based on the publicly available code GADGET-2 (Springel 2005). The hydrodynamics solver uses a pressure–entropy formalism (see Schaller et al. 2015b, for details). The subgrid galaxy formation model includes homogeneous photoionizing background radiation, metallicity-dependent star formation and cooling, stellar evolution and supernovae feedback, seeding and growth of supermassive black holes, and active galactic nucleus (AGN) feedback (see Schaye et al. 2015, for a full description of the model). The galaxy formation model was calibrated to reproduce the stellar mass function of galaxies at $z = 0.1$ and realistic galaxy sizes, down to a stellar mass of $\sim 10^8\,\mathrm{M}_\odot$. The model has been shown to produce galaxies with realistic mass profiles and rotation curves (Schaller et al. 2015a).

We analyse the main EAGLE simulation (Ref0100N1504) that follows the evolution of a periodic cubic volume of $(100\ \mathrm{Mpc})^3$. The mass resolution is $9.6 \times 10^6\,\mathrm{M}_\odot$ and $1.81 \times 10^6\,\mathrm{M}_\odot$ for dark matter and gas particles, respectively. The FRIENDS-OF-FRIENDS (FOF) algorithm was used to identify dark matter haloes (Davis et al. 1985), and the SUBFIND algorithm was used to identify self-bound structures and substructures within the FOF groups (Springel 2005). The cosmological parameters adopted for the simulations are based on Planck Collaboration I (2014): $\Omega_\mathrm{m} = 0.307$, $\Omega_\lambda = 0.693$, $\Omega_\mathrm{bar} = 0.048$, $H_0 = 67.77\,\mathrm{km\,s^{-1}Mpc^{-1}}$,and $\sigma_8 = 0.8288$.

The large volume of the main EAGLE simulation provides a large number of MW-mass galaxies that have a variety of merger histories. The stellar mass, M_*, for each galaxy was calculated by summing the mass of the star particles bound to each galaxy within 30 kpc of the galaxy's centre. The halo mass and radius, M_{200} and R_{200}, respectively, are defined as those of the sphere with average enclosed density equal to 200 times the critical density of the universe (ρ_crit). We define satellites as those subhaloes within R_{200} of their host. Infall time or accretion time is defined as the time when a galaxy crosses the R_{200} radius of the host. In practice, we take the snapshot immediately before the crossing. Finally, merger time is defined as the last snapshot at which an accreted galaxy was identified by SUBFIND, before it merges with the host or is destroyed.

2.2 Sample selection

We first identify all galaxies with a present-day dark matter halo in the mass range $(0.7-2)\times10^{12}\,\mathrm{M}_\odot$ (see Callingham et al. 2019, and references therein). This sample comprises $N = 1078$ haloes. We then impose further restrictions based on assembly history.

The LMC is a relatively massive satellite, $M_* = 1.5\times10^9\,\mathrm{M}_\odot$, with a small Galactocentric distance, $d_{\rm GC} = 50$ kpc, and moves with a large tangential speed (McConnachie 2012; Kallivayalil et al. 2013). The Galactocentric distance and velocity of the LMC indicate that it is close to the pericentre of its orbit. We do not impose any constraint on the orbit of LMC-mass satellites and only require that the stellar mass of the satellite galaxy should lie in the range $(1-4)\times10^9\,\mathrm{M}_\odot$, and the satellite be located within R_{200} of the host halo at $z = 0$. We additionally require that no other satellite more massive than the LMC exists within the R_{200} radius of the MW-mass hosts at $z = 0$. We do not impose a constraint on the infall time of the LMC-mass satellite. However, since these massive satellites survive to $z = 0$, they typically infall at late times.

The details of the GES-like event are more uncertain since it is a fairly new discovery. However, the stellar mass is likely to be in the range $(0.5-1)\times10^9\,\mathrm{M}_\odot$ and it is thought to have merged with the MW between 8 and 11 Gyr ago (Belokurov et al. 2018; Fattahi et al. 2019; Mackereth et al. 2019).[2] We impose no orbital constraint on the GES event. Similarly to the LMC constraint, we require that there was *only one* GES-mass accretion event in this time period (with no merger with a galaxy more massive than the GES). Finally, we impose the conditions that there should be no massive accretion events with progenitor stellar mass $M_* > 0.5\times10^9\,\mathrm{M}_\odot$ in the interval between the GES merger event and the infall of the LMC, and also that there should have been no massive accretion events prior to the accretion of the GES. Our constraints do, however, allow lower mass accretion events such as Sgr and Sequoia to occur between the merger with the GES and the infall of LMC. We do not consider the accretion of a Kraken-like event since it is suspected that this happened before the GES event. A brief summary of the selection criteria are as follows:

(i) MW analogue has $M_{200} = (0.7-2)\times10^{12}\,\mathrm{M}_\odot$.
(ii) LMC exists at $z = 0$ within R_{200}, with stellar mass $M_* = (1-4)\times10^9\,\mathrm{M}_\odot$.
(iii) GES merger event of mass $M_* = (0.5-1)\times10^9\,\mathrm{M}_\odot$ occurs at $t = 8-11$ Gyr.
(iv) A 'merger-free zone' (orange shaded region in Fig. 1) when there are no massive accretion ($M_* > 0.5\times10^9\,\mathrm{M}_\odot$) events between the time of the merger of the GES and the infall of the LMC or prior to the merger with GES.

In order to apply these criteria, we used merger trees to follow the assembly history of the MW-mass galaxies. Fig. 1 shows an example of an MW-mass galaxy in EAGLE, and helps to visualize the constraints imposed by the different selection criteria. The black and orange lines show the main branch of the simulated MW galaxy and its LMC satellite, respectively. The red dots represent dwarf galaxies (above stellar mass of $10^7\,\mathrm{M}_\odot$) that have merged on to the MW main branch, the light red lines show the main branch of the merging dwarfs up until they have completely merged with the MW. The orange and purple shaded regions show the mass and redshift zones for the merger-free area, and the area in which a GES merger should occur.

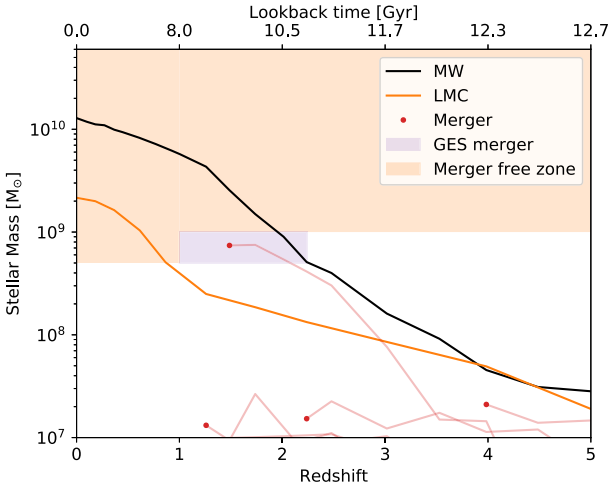

Figure 1. An example of mass growth and merger history of an MW-mass galaxy in EAGLE. The black and orange solid lines show the stellar mass of the main MW progenitor and its LMC satellite from $z = 5$ to $z = 0$. Light red lines correspond to all dwarf galaxies (above stellar mass of $10^7\,\mathrm{M}_\odot$) that merged with the MW halo. Red dots mark the merger time (i.e. the latest snapshot where the progenitors were identified). The orange shaded region illustrates the area which, according to our criteria (Section 2.2), should be merger free. The purple shaded region illustrates the criteria for when a GES merger should occur.

Throughout this paper, the properties of MW-mass galaxies are compared in the 'categories' described below. These groupings were chosen to clarify how having either, or both of the LMC and GES would have influenced the Galaxy's evolution. These categories are:

(i) All MW-mass galaxies (MW-all).
(ii) MW-mass galaxies that have an LMC within R_{200} at $z = 0$ with no merger history constraint. This is the 'classical' MW with LMC studied in many previous papers (LMC-all).
(iii) MW-mass galaxies that have an LMC within R_{200} at $z = 0$, but did not experience a GES merger event or accrete any other massive dwarfs of mass $M_* > 0.5\times10^9\,\mathrm{M}_\odot$ (the 'merger free zone' shown in Fig. 1; LMC-o).
(iv) MW-mass galaxies that have a merger event similar to the GES, but do not have an LMC satellite at $z = 0$ and did not accrete any other massive dwarfs (as in LMC-o; GES-o).
(v) MW-mass galaxies that have both an LMC, a GES event, and a 'merger free zone' during which no object more massive than the LMC or the GES is accreted. This final group (LMC and GES) most closely describes the true MW galaxy.[3]

The number of galaxies that meet these criteria is presented in Table 1, along with the percentage of MW galaxies that belong in each category and their median stellar and halo masses. More details for galaxies in the LMC & GES category are presented in Table 2. Our values for the fraction of MW-mass haloes in the LMC-o or GES-o categories are significantly higher than those stated in Bignone et al. (2019) and Cautun et al. (2019). Cautun et al. (2019) found only eight MW analogues in the EAGLE simulation which had an LMC-mass satellite; however, that work applied more restrictive constraints to the sample. For example, the mass of the cold gas content and the

[2]Fattahi et al. (2019) find a slightly higher stellar mass for the GES progenitors in the Auriga simulations. However, the stellar masses in Auriga subhaloes are slightly overestimated.

[3]Kruijssen et al. (2020) found a lower mass for the GES than used in this paper. However, their findings for the MW assembly history are consistent with the LMC-o sample of galaxies presented here.

Table 1. Details of the MW-mass galaxies included in our sample.

Group	Number of galaxies	Percentage	Median M_* ($\times 10^{10}$ M$_\odot$)	Median M_{200} ($\times 10^{12}$ M$_\odot$)	M_*/M_{200} ($\times 10^{-3}$)	MAD M_* ($\times 10^{9}$ M$_\odot$)	MAD M_{200} ($\times 10^{11}$ M$_\odot$)
MW-all	1078	–	2.03	1.04	19.5	9.03	3.48
LMC-all	169	15.7	1.78	1.12	15.9	9.83	4.25
LMC-o	40	3.7	1.30	0.87	14.9	7.12	2.11
GES-o	54	5.0	1.74	0.92	18.9	5.68	1.97
LMC and GES	7	0.65	1.44	0.80	18.0	7.13	0.53

Table 2. The final sample of 7 MW analogues with LMC and GES. The columns give: (a) EAGLE halo ID, corresponding to the halo ID in the top left of Fig. 3; (b) M_{200} of the MW halo at $z = 0$; (c) the maximum stellar mass recorded for the destroyed GES; (d) the redshift at which the GES merged; (e) maximum stellar mass of the LMC analogue; (f) redshift at which the LMC analogue crossed the R_{200} radius of the MW; and (g) the number of satellites within R_{200} of the MW analogues with stellar mass, $M_* > 10^6$ M$_\odot$.

EAGLE Halo ID (a)	MW M_{200} ($\times 10^{12}$ M$_\odot$) (b)	GES $M_{*,\,\mathrm{max}}$ ($\times 10^{8}$ M$_\odot$) (c)	GES merger redshift (d)	LMC $M_{*,\,\mathrm{max}}$ ($\times 10^{9}$ M$_\odot$) (e)	LMC infall redshift (f)	Number of satellites (g)
8806615	1.13	5.2	2.01	2.16	0.37	6
9293658	0.99	5.4	1.00	1.29	0.27	8
9372228	0.76	7.4	1.49	2.16	0.27	9
9626514	0.80	6.2	1.00	1.26	0.1	13
9798319	0.80	9.0	1.74	1.27	0.74	12
9968042	0.79	7.8	1.00	1.46	0.37	6
10058549	0.71	9.9	1.26	3.34	0.62	10

black hole mass were also considered in the constraints. Bignone et al. (2019) found only one MW galaxy with a GES type merger event in the EAGLE simulation; however, that work also imposed constraints on the current star formation and the disc of the MW, and, importantly, required that the stellar debris from the GES event be highly anisotropic.

Our constraints are deliberately imposed to depend only on the mass and time of significant accretion events in the MW's history. Anything more restrictive would result in a very small sample size. The fraction of MW haloes with 'classical' LMCs (LMC-all) is slightly higher than the observed value ($\sim$ 10 per cent; see e.g. Liu et al. 2011; Tollerud et al. 2011) but, again, our constraints are less restrictive (e.g. no constraint on present-day position, or orbit of the LMC). The final value for the fraction of MW galaxies with both an LMC and a GES merger event, and nothing significant in between, is only 0.65 per cent of all MWs in EAGLE – this is already an indicator that our Galaxy's assembly history is very rare.

Four representative galaxies from our final LMC and GES sample are illustrated in Figs 2 and 3. The former shows mock *gri* face-on images of the central galaxies at $z = 0$, where face-on has been defined according to the stellar angular momentum axis (Trayford et al. 2017).[4] The images have been retrieved from the EAGLE public data base.[5] They have been produced by post-processed ray tracing using a version of the code SKIRT (Camps & Baes 2015); please see Trayford et al. (2017) for more details. Fig. 3 shows 2D projections of the dark matter particles in a (500 kpc)^3 region around the four haloes. The outer and inner circles mark the R_{200} and $0.5 \times R_{200}$ boundaries. The LMC-mass satellite is highlighted in each halo with a red circle.

[4]Note that Trayford et al. (2017) state that the galactic plane is not always easily defined, which could explain the irregularity of the leftmost image in Fig. 2

[5]http://virgodb.dur.ac.uk:8080/Eagle/

3 RESULTS

We now present an overview of the properties of our various MW-mass categories defined in the previous section and their assembly histories. We start by examining the stellar and halo mass distributions and the stellar mass–halo mass relation.

The halo mass distributions of our different MW-mass categories are displayed in the top panel of Fig. 4. The black line shows the distribution of halo masses for the MW-all sample. The mass distributions are approximately linear, with a slight bias towards lower mass haloes, as expected from the power-law halo mass function in ΛCDM in this mass range (Jenkins et al. 2001). The decrease in halo mass distributions at the lowest mass bins is an artefact introduced by the KDE kernel used for smoothing. The LMC-all sample (dashed orange line) follows the general MW-mass halo trend closely, although it is flatter and less biased towards lower masses. This classical LMC-all group is different from the LMC-o group shown as the solid orange line, which has a more prominent peak towards lower masses.

Fig. 4 shows that the halo mass of the MW is shifted towards lower values for both the LMC-o and GES-o samples (medians of 0.87×10^{12} M$_\odot$ and 0.92×10^{12} M$_\odot$, respectively). This effect is further enhanced when the MW has both an LMC and a GES. The halo masses for the LMC-o and GES-o groups are biased low because they have a long quiescent period and thus, compared to the 'typical' MW, have accreted less mass. The seven LMC and GES galaxies are represented individually by vertical dashed red lines. Halo mass, by definition, is all the mass within R_{200} and therefore includes the halo mass of the LMC-mass satellite.

The stellar mass–halo mass relationship is shown in the central panel of Fig. 4. The LMC-all and LMC-o samples appear to have

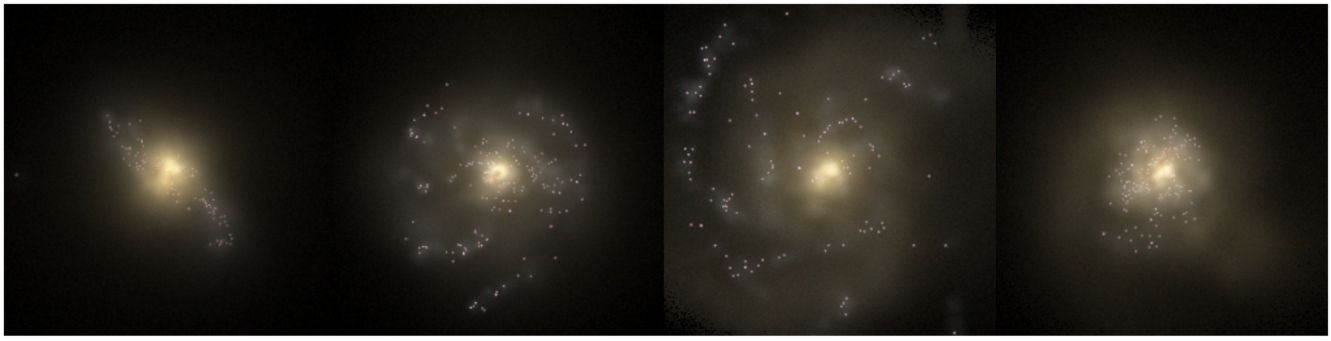

Figure 2. Composite face-on *gri* images of four representative MW-mass galaxies in our final sample (LMC and GES) from the EAGLE reference simulation. Each panel is 60 × 60 pkpc wide. Details of the visualization can be found in Trayford et al. (2017). Left to right, the EAGLE halo ID's are 9293658, 9372228, 9798319, and 10058549.

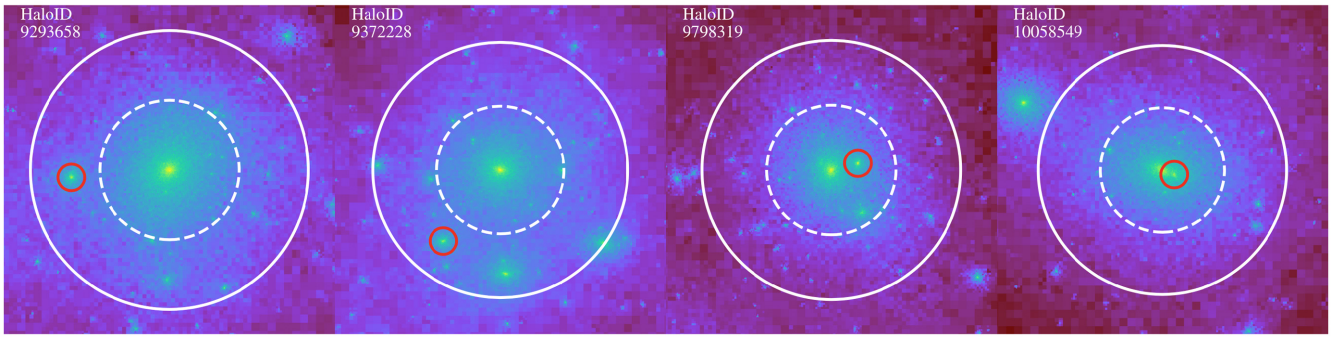

Figure 3. Distribution of dark matter particles for the corresponding galaxies shown in Fig. 2. The solid and dashed white circles represent the host R_{200} and $0.5 \times R_{200,}$ respectively. The smaller red circle shows the location of the LMC satellite. The EAGLE halo ID is shown in the top left-hand corner of each halo.

a lower stellar mass compared to the total sample at any given halo mass. We, however, note that there are biases in the way halo and stellar masses are measured. The stellar mass includes the stellar particles within 30 kpc of the centre of the MW; however, the halo mass, M_{200}, includes all mass within the FOF group (i.e. including the halo of the LMC that is generally more than 30 kpc away from the centre). Therefore, the difference is not a shift down in stellar mass for MWs with an LMC but rather a shift to the right in the stellar mass–halo mass plane.

The central panel of Fig. 4 suggests that the GES-o category has a higher than average stellar mass for a given halo mass in the range $\log_{10}(M_{200}) = 11.9 - 12.1$. However, the stellar mass distribution shown in the right-hand panel shows that there is a small peak at slightly higher stellar mass for the GES-o sample than the average MW peak, but the main peak for the GES-o sample is at a slightly lower stellar mass than the average. This is because this category is biased towards lower halo masses (see top panel), and thus lower, on average, stellar masses. For low halo masses [$\log_{10}(M_{200}) < 12$], the LMC and GES sample has lower than average stellar mass, but for higher halo masses [$\log_{10}(M_{200}) > 12$], it has higher than average stellar mass. However, the median relation in this mass range remains within the median absolute deviation of the MW-all category (shaded grey region). The former is due to the aforementioned reason for LMC samples; namely, the stellar mass is measured for the central galaxy but halo mass includes the mass of LMC.

The right-hand panel of Fig. 4 shows the distribution of stellar masses for each category of galaxies. The LMC-o sample has a peak at lower stellar masses than the MW-all sample, reflecting the lower halo masses seen in the top panel. The stellar masses of the LMC and GES sample are distributed across the entire range of stellar masses.

3.1 Assembly history

Fig. 5 shows the evolution of stellar mass (left-hand panel), M_{200} (middle panel), and the normalized halo mass ($M_{200}/M_{200,\,z=0}$; right-hand panel) for each category of MW-mass galaxies. The thick lines show the median stellar mass and halo mass at each redshift for each sample.

The LMC-all category (dashed orange line) does not have any constraint on assembly history and is consistently lower in stellar and halo mass until the infall of its LMC-mass satellite. During infall, the LMC satellite gives rise to a sudden increase in halo mass, which leads to the LMC-all sample having the highest halo mass of all categories at $z = 0$. The LMC-o sample is consistently low in both stellar and halo mass. As in the case of the LMC-all sample, the LMC-o galaxies also show an increase in halo mass as the LMC-mass satellite is accreted by its host. However, unlike the LMC-all sample, the final halo masses are not particularly high, and, in fact, are lower on average than the MW-all sample. This difference reflects the fact that the LMC-o sample is constrained to have no other significant merger (other than the LMC), which naturally biases this sample to lower halo masses.

The GES-o group follows the MW-all sample more closely than the LMC samples. However, the stellar and halo masses of the GES-o category tend to grow more rapidly around the time of the GES merger, and this shows up as a 'bump' in the central and right-hand panels of Fig. 5 around $z \sim 1$–2. Preceding this event, the stellar and halo mass rise more slowly than the average MW sample since the MW-all sample experiences more continuous mergers than the GES-o, and therefore has a continuous influx of accreted mass.

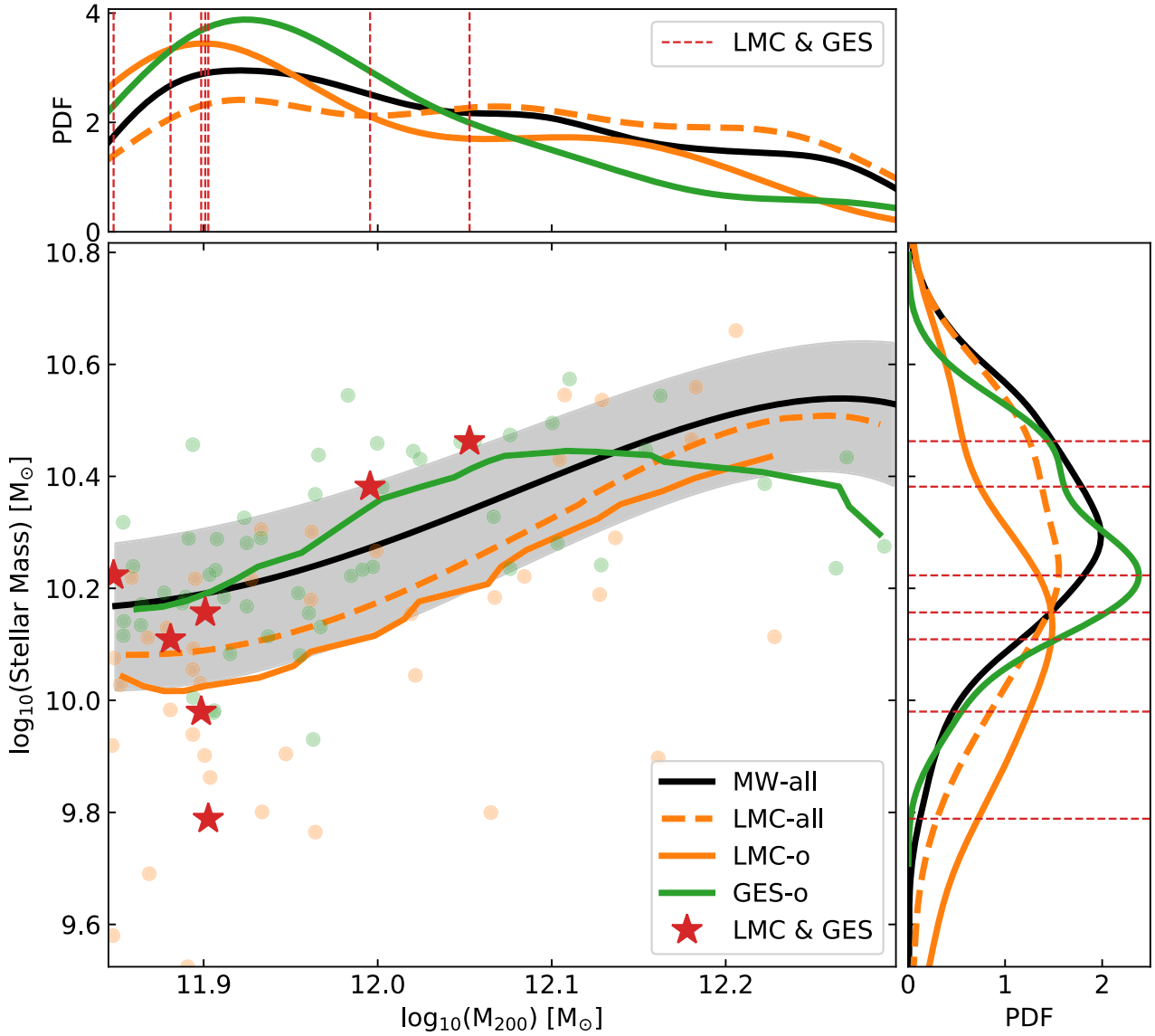

Figure 4. *Central:* stellar mass–halo mass relation at $z = 0$ for our different samples of MW-mass haloes (see Section 2.2 for full details), as indicated in the legend. The lines represent the median values of the stellar mass in halo mass intervals. For the 'MW-all' sample, we show the median absolute deviation (MAD) around the median as a shaded region, whereas for the other samples we show individual galaxies with the corresponding colour. The medians and the MAD were smoothed using a Savitzky–Golay filter (Savitzky & Golay 1964). The red stars correspond to the individual galaxies in the final sample of MWs with LMC and GES. *Top:* M_{200} distribution of various MW-mass samples, smoothed with a KDE kernel. Vertical lines indicate individual galaxies in our LMC and GES sample. *Right:* similar to the top panel but showing the stellar mass distribution of MW-mass haloes.

Initially, the LMC and GES galaxies have stellar and halo masses that are lower than those of the LMC-o sample. These galaxies then follow the evolution of the LMC-o category until the merger with the GES at $z = 1$–2, when it also shows a bump in halo mass similar to that in the GES-o category. Some of the individual LMC and GES galaxies show a very sudden increase in halo mass (in some cases almost double in mass) because of the accretion of the LMC-mass satellite. The stellar mass growth is much smoother than the halo mass growth. There is no bump in the stellar mass corresponding to the bump in halo mass since not all stars go to the centre of the MW (i.e. within 30 kpc, the aperture used to calculate the stellar mass). Evidently, the progenitors of the LMC and GES galaxies are considerably smaller than the other categories of MW-mass galaxies. The combination of the two events, the merger with the GES and the infall of the LMC, increases the halo mass of their MW galaxies enough to reach our minimum mass threshold. Hence, our results suggest that the main progenitor of the MW would have been much smaller than anticipated.

The difference in the assembly histories of our various MW categories is more apparent in the right-hand panel of Fig. 5, which shows the normalized halo mass as a function of redshift. There is a clear bump in the GES-o sample (green line) around the redshift of the GES merger with the MW. There is also clearly a sudden increase in halo mass of the LMC-o sample (solid orange line) at infall time of the LMC-mass satellite. Some of the LMC and GES individual galaxies (red dashed lines) go above $M_{200}/M_{200,\,z=0} = 1$, which is likely due to the definition of M_{200}. When a massive object such as the LMC is close to the virial radius (i.e. infalling),

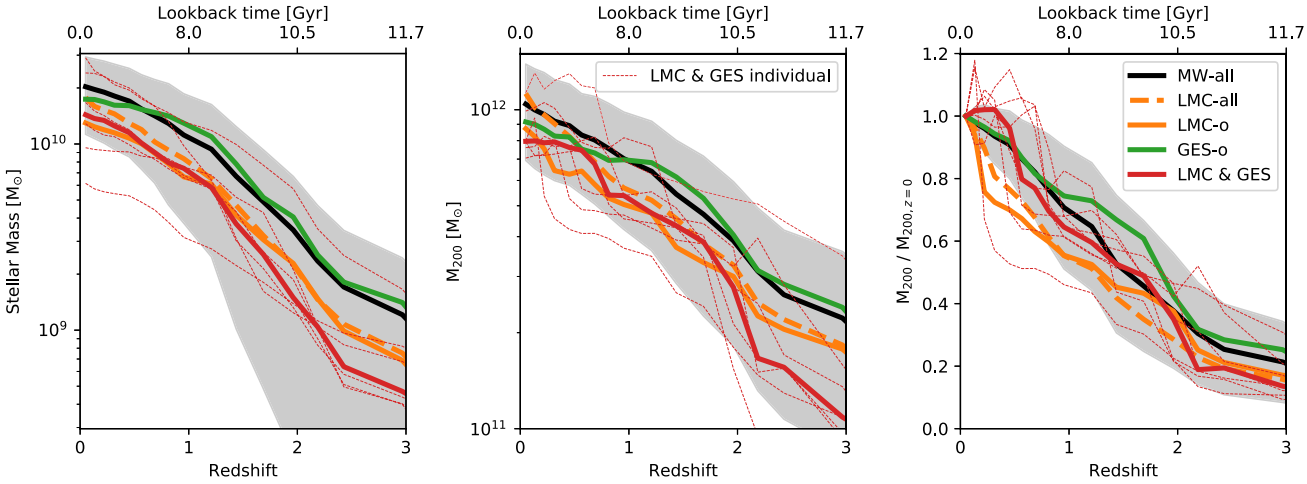

Figure 5. *Left:* median stellar mass as a function of redshift for different MW-mass samples. The colour coding and line styles are similar to those in Fig. 4. The shaded region represents the MAD around the median for the MW-all sample. The thin red dotted lines correspond to individual galaxies in the final LMC and GES sample. *Middle:* as the left-hand panel, but for the halo mass, M_{200}, as a function of redshift. *Right:* as the middle panel, but for the halo masses normalized to the $z = 0$ value for each halo, as a function of redshift.

R_{200} is not very well defined and tends to increase in order for the mean density to drop to 200 $\times$ $\rho_{\rm crit}$. As a consequence, the mass in the boundary region also contributes to M_{200}, and this temporarily increases. After infall, LMC-mass subhaloes quickly sink to the centre, and R_{200} (and thus M_{200}) goes back to 'normal'. Thus, the transient increase in M_{200} does not mean the MW-mass haloes lose mass, but rather is a result of the definition of R_{200} and the accretion of massive subhaloes. This feature is averaged out in the LMC-all and LMC-o samples due to the greater range of infall times for the LMC.

We use the normalized halo mass assembly to define halo formation redshifts, z_X, for each MW-mass galaxy as the time when the main progenitor branch of the merger tree reaches X percent of the present-day M_{200}. Fig. 6 shows z_{25}, z_{50}, and z_{75} of our MW samples in the left-hand, middle and right-hand panels, respectively.

Due to the sudden increase in halo mass resulting from the infall of the LMC-mass satellite, the formation redshifts of the LMC-all and LMC-o categories are shifted to lower values across all three panels. The z_{75} formation redshift is the most affected by this since this is roughly the infall time of the LMC-like satellites, particularly for the lower halo mass galaxies.

The GES-o sample has a consistently earlier formation redshifts across all three panels. The left-hand panel suggests that the GES-o galaxies form 25 per cent of their mass earlier than the other samples even before the merger with the GES. The middle panel shows that the z_{50} formation redshift occurs at roughly the same redshift as the merger with the GES, and the right-hand panel shows that after the merger with the GES, the GES-o galaxies follow the MW-all sample more closely.

Overall, Fig. 6 suggests that the LMC and GES galaxies tend to have later z_{25} formation redshifts, similar to the LMC-o formation redshifts. This is expected since in that time interval the GES is only beginning to merge with the MW and so the galaxy has experienced roughly the same amount of merging as the LMC-o category. The middle panel shows that the z_{50} formation redshifts of the LMC and GES follow more closely the GES-o line, which is likely due to the merger of the GES occurring at roughly these redshifts. Finally, the right-hand panel shows that the lower mass ($M_{200} < 10^{12}\,{\rm M}_\odot$) LMC and GES return to follow the LMC-o lines for the z_{75} formation redshifts, likely due to the imminent infall of the LMC-like satellites.

The two higher mass LMC and GES galaxies ($M_{200} > 10^{12}\,{\rm M}_\odot$) do not follow the same trend as the lower mass galaxies at this epoch. This is likely because the accretion of the LMC-mass satellite is a proportionally larger accretion event for the lower mass LMC and GES galaxies. Figs 5 and 6 show that the assembly history of the MW intricately follows the details of these two (GES and LMC) accretion events, and, at most redshifts, looks very different to the average MW-mass halo.

3.2 Galaxy colour and morphology

Assembly histories are reflected in the morphology of galaxies. Our selection of samples of MW-mass galaxies with different constraints (Section 2.2) does not include any criteria for the MW to be a star-forming spiral galaxy rather than a red, non-star forming elliptical galaxy. In this section, we show how the assembly history affects the $z = 0$ colours of our galaxies.

To characterize the MW-mass galaxies, we consider their colour and morphology. The rest-frame absolute magnitude without dust attenuation was used to estimate the colour; see Trayford et al. (2015) for details. We adopt the threshold defined by Schawinski et al. (2014) to label galaxies as blue or red (dashed line in Fig. 7). The fraction of blue galaxies for the MW-all sample is $f_{\rm blue} = 0.82$.

Fig. 7 shows the colour–stellar mass diagram for our MW-mass haloes. The grey contours, repeated in all panels, correspond to the distribution for the MW-all group which is clearly bimodal showing a red sequence and a blue cloud. Different panels correspond to the various categories of MW-mass galaxies, as labelled, with the colour of each point indicating whether they are disc (blue) or elliptical (red) galaxies. To characterize morphology, we use the stellar kinematics morphological indicator introduced by Sales et al. (2012) and calculated for EAGLE galaxies by Correa et al. (2017). The fraction of disc galaxies (i.e. with $\kappa_{\rm co} \geq 0.4$) for the MW-all sample is 0.6.

The left-hand panel shows that the LMC-o sample contains more blue galaxies than average, with $f_{\rm blue} = 0.9$. This is likely due to the late formation redshift discussed previously, and the restriction that there should be no significant mergers until the LMC infall. However, fewer galaxies in the LMC-o sample are disc galaxies compared to the MW-all sample. This slightly lower disc fraction

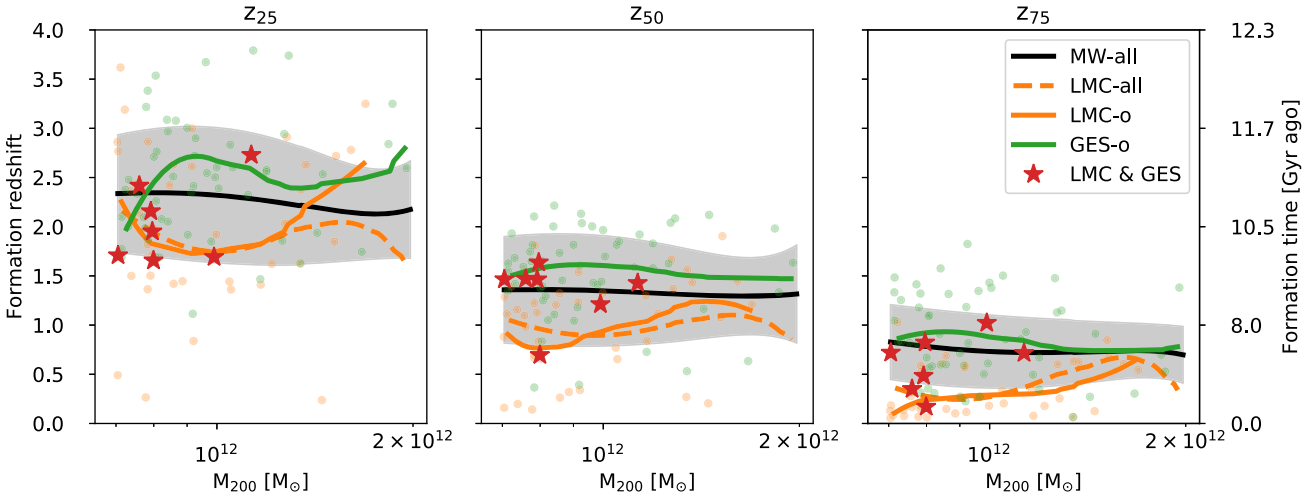

Figure 6. The formation redshifts of the MW-mass haloes. *Left:* redshift when the halo has reached 25 per cent of its $z = 0$ mass. *Middle:* redshift when the halo has reached 50 per cent of its $z = 0$ mass. *Right:* redshift when the halo has reached 75 per cent of its $z = 0$ mass. Colours, lines, and symbols are similar to those of Fig. 4. The black line represents the median value of the redshifts for the MW-all category, and the grey shaded region represents the MAD for that category. The median lines were smoothed using a Savitzky–Golay filter.

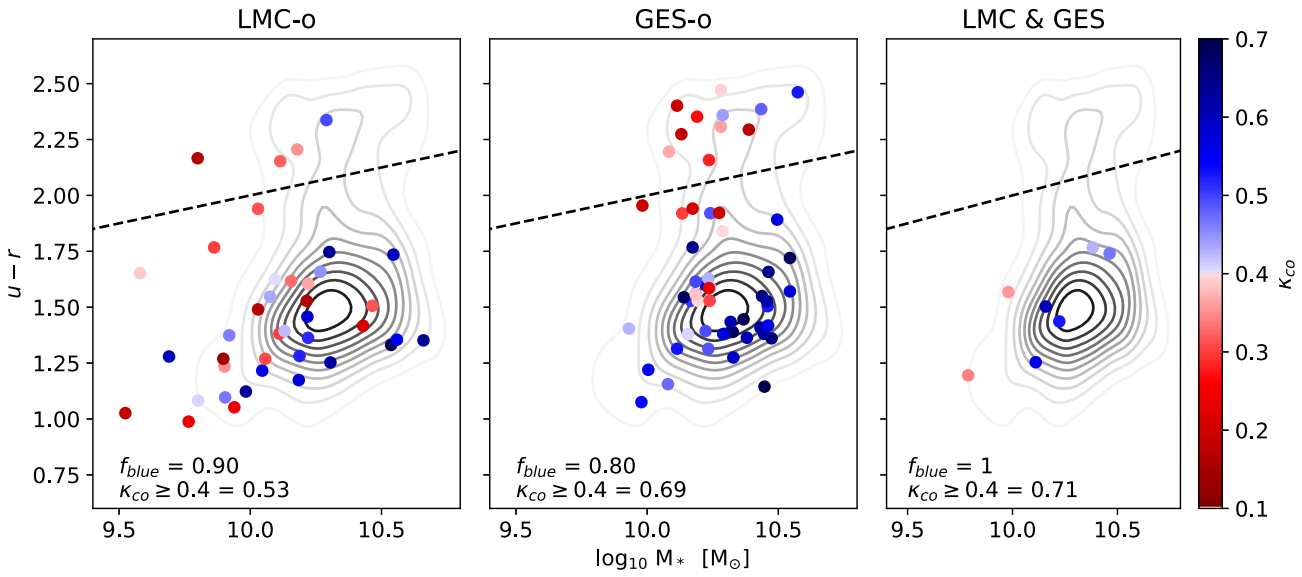

Figure 7. The $u - r$ colour *versus* stellar mass diagram for MW-mass galaxies. The panels correspond to the LMC-o (left), GES-o (middle), and LMC and GES (right) samples. The grey contours are repeated in all panels and show the colour–stellar mass distribution for the 'MW-all' sample. Galaxies are represented by red or blue according to a cut in their $\kappa_{\rm co}$ values at $\kappa_{\rm co} = 0.4$, as shown by the colour bar. The dashed black line marks the separation of the red sequence from the blue cloud. The legend gives the fraction of blue galaxies ($f_{\rm blue}$) and the fraction of disc galaxies ($\kappa_{\rm co} \geq 0.4$).

is likely due to the LMC-o sample galaxies having lower stellar masses than average (see Fig. 4). In addition, some of the discs could have been disturbed by the infalling LMC. The middle panel shows that the GES-o sample contains a similar fraction of blue galaxies as the MW-all sample but a much higher fraction of disc galaxies. Since GES-o galaxies experience an early merger event (and hence have an earlier formation redshift) they are more likely to become redder with time. The right-hand panel shows that the LMC and GES galaxies are all in the blue cloud. This is consistent with the trend seen in the LMC-o sample that the later forming galaxies are more likely to be bluer. The LMC and GES sample also has the highest fraction of disc galaxies, 0.71, similar to the GES-o sample.

3.3 Satellite population

In this subsection, we examine the satellite population of our MW samples and investigate whether the LMC and GES sample is different in this respect to the other samples. As shown in the simulations of the APOSTLE project (Fattahi et al. 2016; Sawala et al. 2016), the EAGLE model reproduces well the observed stellar mass function for dwarf galaxies, both those that are satellites orbiting in the MW and those in the field around the Local Group. Several important properties of dwarf galaxies, such as their sizes and star formation histories, are also consistent with observations (Sales 2016; Sawala et al. 2016; Campbell et al. 2017; Digby et al. 2019; Bose et al. 2019, 2020).

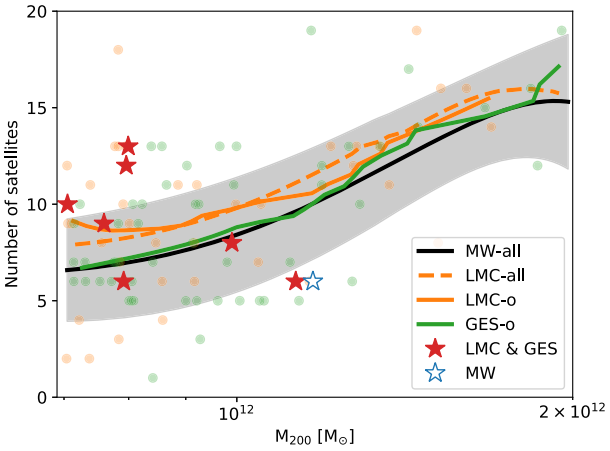

Figure 8. Number of satellites of stellar mass, $>1 \times 10^6$ $M_\odot$, within the radius R_{200} for the host, as a function of host halo mass, M_{200}, for various samples of MW-mass galaxies. The colours, lines, and shading are similar to those in Fig. 4. The blue open star shows the number of Galactic satellites with stellar mass above 10^6 $M_\odot$. R_{200} and M_{200} for the MW halo have been taken from Callingham et al. (2019).

The number of 'luminous' satellites as a function of halo mass for our various samples is shown in Fig. 8. Since EAGLE does not resolve ultra-faint dwarfs, the satellites plotted are those with stellar mass above $M_* > 1 \times 10^6$ $M_\odot$ that are within the virial radius of the MW-mass haloes. The mass and number of satellites above this stellar mass within the M_{200} radius of our Galaxy is shown as a blue open star symbol. Here, the halo mass of the MW and its R_{200} radius are taken from Callingham et al. (2019) and the stellar masses and Galactocentric distances of the MW satellites from McConnachie (2012). The number of satellites with $M_* > 1 \times 10^6$ $M_\odot$ around MW-like galaxies is in agreement with other hydrodynamical simulations (e.g. Okamoto et al. 2010; Zolotov et al. 2012; Sawala et al. 2016; Wetzel et al. 2016; Simpson et al. 2018; Garrison-Kimmel et al. 2019).

Fig. 8 shows the well-known correlation between the number of satellites and the halo mass (Wang et al. 2012). The LMC-all and LMC-o samples have slightly higher numbers of satellites at fixed halo mass than the MW-all sample. This is probably because the LMC-mass dwarfs would have brought in their own satellite cohorts (Shao, Cautun & Frenk 2019). The GES-o sample has a very similar trend to the MW-all sample, possibly because these galaxies have a similar late-time assembly history to the MW-all galaxies (Fig. 5 right-hand panel) when the bulk of the satellite population is accreted (Fattahi et al. 2020). At low halo masses, the infall of the LMC-like satellite (in LMC-all, LMC-o, and LMC and GES samples) has a much larger impact as it is fractionally much larger compared to the host than for higher halo mass MW galaxies. We also examined the radial distribution of satellites and found no discernible differences between the different categories of MW-like galaxies. However, we note that we do not take 'orphan' satellites into consideration, which can make a substantial difference to the radial profiles (Bose et al. 2020).

4 DISCUSSION AND CONCLUSIONS

We have used the EAGLE hydrodynamical simulation to assess the extent to which the two known major accretion events experienced by our Galaxy – the GES merger at early times and the more recent infall of the LMC – have shaped the properties of our galaxy. We have also tested whether these events make the MW stand out among galaxies of similar mass.

We identified 1078 MW-mass haloes in the mass range $M_{200} = (0.7 - 2) \times 10^{12}$ $M_\odot$ and subdivided this sample into three: (i) galaxies with an LMC-mass satellite within their virial radius at $z = 0$ (LMC-all sample); (ii) galaxies with an LMC as in (i), but which did not experience a GES merger event or accrete any other more massive dwarfs than that in the past 8 Gyr (LMC-o sample); (iii) galaxies that experienced a merger between $z = 1$–2 similar to the GES but no further large mergers (GES-o sample); and (iv) galaxies that experienced both a GES merger and the accretion of an LMC-mass satellite but no other significant mergers in between these two (LMC and GES sample). Only seven galaxies fall in the last category; their assembly histories bear the closest resemblance to the assembly history of the MW, as far as it is currently known. Our main conclusions are as follows:

(i) In agreement with earlier work, we find that the presence of an LMC-mass satellite orbiting an MW-mass galaxy is relatively uncommon: only 15.7 per cent of galaxies fall in our LMC-all category. However, once the constraint is imposed that there should have been no massive mergers in the past 8 Gyr, the frequency is reduced to 3.7 per cent (LMC-o). The number of MW-mass galaxies with a GES event between $z = 1$–2 (GES-o) amounts to 5 per cent of the total sample. These fractions are slightly higher than in other studies (e.g. Bignone et al. 2019; Cautun et al. 2019) because of different ways of identifying the LMCs and GES in simulations.

(ii) The assembly history of the MW is rare in the ΛCDM model: only 0.65 per cent of MW-mass EAGLE galaxies have both an early GES merger and a late LMC infall and no significant mergers in between. This sample most closely resembles the assembly history of the MW.

(iii) The existence of an LMC or a GES event selects haloes towards the lower end of the mass range we considered. Requiring both events further lowers the halo mass. The bias towards lower halo masses for these samples is due to a long period of quiescence during which the haloes did not accrete as much mass as a 'typical' MW galaxy.

(iv) At a fixed halo mass, galaxies with an LMC (with or without the restriction on past mergers) have lower than average stellar mass. This bias is partly a matter of definition since the stellar mass of the galaxy is measured within 30 kpc, well inside the position of a typical LMC, whereas the mass of the halo is measured out to R_{200}.

(v) Haloes destined to accrete an LMC have lower than average mass at early times but 'catch up' at late times once the LMC has been accreted. The GES-o sample closely follows the accretion history of the MW-all sample until the merger with the GES around $z = 2$. The halo mass grows more rapidly during the GES event ($z \sim 1$–2); after that the increase in halo mass is slower. Haloes in the LMC and GES sample have much lower initial masses but they experience large increases in mass at the time of the merger with the GES and the later infall of the LMC. As a result, the formation redshift of the LMC and GES haloes (defined as the time when 50 per cent of the final halo mass was in place) ends up being typical of haloes of that mass.

(vi) Although no constraints on the morphology, colour or star formation rate of the final galaxy were applied in the sample selection, the LMC and GES galaxies all fall in the 'blue cloud' in the colour–stellar mass diagram. This is a reflection of the long period without massive mergers required for this sample. Using a kinematical diagnostic of galaxy morphology (the fraction of the

kinetic energy invested in rotation), the LMC and GES galaxies are predominantly disc galaxies: whereas 60 per cent of the MW-all sample are discs according to this definition, 70 per cent of the LMC and GES sample are discs.

(vii) Galaxies with an LMC have more satellites than galaxies without one, including those with a GES event. The excess is due to the additional satellite population brought into the MW halo by the LMC.

Our simulations indicate that the build-up of both the stellar and dark matter mass in the MW was strongly influenced by the GES merger and the accretion of the LMC. We therefore expect the progenitors of the MW, perhaps accessible to observational study with forthcoming telescopes such as JWST, to be atypical of galaxies of similar mass today.

The main limitation of this work is the relatively small volume sampled by the EAGLE simulation: there are only seven galaxies in the EAGLE volume that satisfy the main constraints we imposed for the assembly history to resemble that of the MW, namely an early GES merger, a late LMC infall and a quiescent phase in between. A larger simulation is required to understand in more detail the atypical properties of the assembly history of the MW.

ACKNOWLEDGEMENTS

We thank an anonymous referee for helpful comments that allowed us to improve this paper. TE was supported by a Royal Society Research Grant, and AD by a Royal Society University Research Fellowship. AF wass supported by Durham University's International Junior Research Fellowship which received funding from European Union's Marie-Curie COFUND scheme (grant agreement no. 609412). CSF was supported by ERC Advanced Investigator grant, DMIDAS (GA 786910). We acknowledge support by the Science and Technology Facilities Council (STFC) (grant numbers ST/T000244/1 and ST/P000541/1). This work used the DiRAC Data Centric system at Durham University, operated by the ICC on behalf of the STFC DiRAC HPC Facility (www.dirac.ac.uk). This equipment was funded by BIS National E-infrastructure capital grant ST/K00042X/1, STFC capital grant ST/H008519/1, and STFC DiRAC Operations grant ST/K003267/1 and Durham University. DiRAC is part of the National E-Infrastructure. This research made use of the open source project `yt` (Turk et al. 2010).

DATA AVAILABILITY

The data underlying this article are available in the EAGLE online data base, at http://virgodb.dur.ac.uk:8080/Eagle.

REFERENCES

Abadi M. G., Navarro J. F., Steinmetz M., 2006, MNRAS, 365, 747
Amorisco N. C., 2017, MNRAS, 464, 2882
Bell E. F., Monachesi A., Harmsen B., de Jong R. S., Bailin J., Radburn-Smith D. J., D'Souza R., Holwerda B. W., 2017, ApJ, 837, L8
Belokurov V., Erkal D., Evans N. W., Koposov S. E., Deason A. J., 2018, MNRAS, 478, 611
Benson A. J., Frenk C. S., Lacey C. G., Baugh C. M., Cole S., 2002, MNRAS, 333, 177
Bignone L. A., Helmi A., Tissera P. B., 2019, ApJ, 883, L5
Bose S. et al., 2019, MNRAS, 486, 4790
Bose S., Deason A. J., Belokurov V., Frenk C. S., 2020, MNRAS, 495, 743
Boylan-Kolchin M., Bullock J. S., Kaplinghat M., 2011, MNRAS, 415, L40
Bullock J. S., Johnston K. V., 2005, ApJ, 635, 931
Busha M. T., Marshall P. J., Wechsler R. H., Klypin A., Primack J., 2011, ApJ, 743, 40
Callingham T. M. et al., 2019, MNRAS, 484, 5453
Campbell D. J. R. et al., 2017, MNRAS, 469, 2335
Camps P., Baes M., 2015, Astron. Comput., 9, 20
Cautun M., Deason A. J., Frenk C. S., McAlpine S., 2019, MNRAS, 483, 2185
Conroy C., Naidu R. P., Zaritsky D., Bonaca A., Cargile P., Johnson B. D., Caldwell N., 2019, ApJ, 887, 237
Cooper A. P. et al., 2010, MNRAS, 406, 744
Correa C. A., Schaye J., Clauwens B., Bower R. G., Crain R. A., Schaller M., Theuns T., Thob A. C. R., 2017, MNRAS, 472, L45
Crain R. A. et al., 2015, MNRAS, 450, 1937
Davis M., Efstathiou G., Frenk C. S., White S. D. M., 1985, ApJ, 292, 371
Deason A. J., Belokurov V., Sanders J. L., 2019, MNRAS, 490, 3426
Digby R. et al., 2019, MNRAS, 485, 5423
Eggen O. J., Lynden-Bell D., Sandage A. R., 1962, ApJ, 136, 748
Elias L. M., Sales L. V., Helmi A., Hernquist L., 2020, MNRAS, 495, 29
Evans N. W., 2020, in Valluri M., Sellwood J., eds, Proc. IAU Symp. 353, Galactic Dynamics in the Era of Large Surveys. Cambridge Univ. Press, Cambridge, p. 113
Fattahi A. et al., 2016, MNRAS, 457, 844
Fattahi A. et al., 2019, MNRAS, 484, 4471
Fattahi A., et al., 2020, preprint (arXiv:2002.12043)
Font A. S., Johnston K. V., Bullock J. S., Robertson B. E., 2006, ApJ, 646, 886
Fragkoudi F. et al., 2020, MNRAS, 494, 5936
Garavito-Camargo N., Besla G., Laporte C. F. P., Johnston K. V., Gomez F. A., Watkins L. L., 2019, ApJ, 884, 51
Garrison-Kimmel S. et al., 2019, MNRAS, 487, 1380
Gomez F. A., Besla G., Carpintero D. D., Villalobos A., O'Shea B. W., Bell E. F., 2015, ApJ, 802, 128
Harmsen B., Monachesi A., Bell E. F., de Jong R. S., Bailin J., Radburn-Smith D. J., Holwerda B. W., 2017, MNRAS, 466, 1491
Helmi A., Babusiaux C., Koppelman H. H., Massari D., Veljanoski J., Brown A. G. A., 2018, Nature, 563, 85
Jenkins A., Frenk C. S., White S. D. M., Colberg J. M., Cole S., Evrard A. E., Couchman H. M. P., Yoshida N., 2001, MNRAS, 321, 372
Kallivayalil N., Marel R. P. v. d., Besla G., Anderson J., Alcock C., 2013, ApJ, 764, 161
Kruijssen J. M. D., Portegies Zwart S. F., 2009, ApJ, 698, L158
Kruijssen J. M. D. et al., 2020, preprint (astro-ph/2003.01119)
Laporte C. F. P., Gómez F. A., Besla G., Johnston K. V., Garavito-Camargo N., 2018, MNRAS, 473, 1218
Libeskind N. I., Frenk C. S., Cole S., Helly J. C., Jenkins A., Navarro J. F., Power C., 2005, MNRAS, 363, 146
Liu L., Gerke B. F., Wechsler R. H., Behroozi P. S., Busha M. T., 2011, ApJ, 733, 62
Lynden-Bell D., 1976, MNRAS, 174, 695
McAlpine S. et al., 2016, Astron. Comput., 15, 72
McConnachie A. W., 2012, AJ, 144, 4
Mackereth J. T. et al., 2019, MNRAS, 482, 3426
Metz M., Kroupa P., Libeskind N. I., 2008, ApJ, 680, 287
Myeong G. C., Evans N. W., Belokurov V., Sanders J. L., Koposov S. E., 2018, ApJ, 863, L28
Myeong G. C., Vasiliev E., Iorio G., Evans N. W., Belokurov V., 2019, MNRAS, 488, 1235
Okamoto T., Frenk C. S., Jenkins A., Theuns T., 2010, MNRAS, 406, 208
Penarrubia J., Walker M. G., Gilmore G., 2009, MNRAS, 399, 1275
Penarrubia J., Gómez F. A., Besla G., Erkal D., Ma Y.-Z., 2016, MNRAS, 456, L54
Pfeffer J. L., Trujillo-Gomez S., Kruijssen J. M. D., Crain R. A., Hughes M. E., Reina-Campos M., Bastian N., 2020, preprint (arXiv:2003.00076)
Planck Collaboration I, 2014, A&A, 571, A1
Sales L., 2016, HST Proposal, #14582
Sales L. V., Navarro J. F., Theuns T., Schaye J., White S. D. M., Frenk C. S., Crain R. A., Dalla Vecchia C., 2012, MNRAS, 423, 1544
Savitzky A., Golay M. J. E., 1964, Anal. Chem., 36, 1627

Savorgnan G. A. D., Graham A. W., Marconi A., Sani E., 2016, ApJ, 817, 21
Sawala T. et al., 2016, MNRAS, 457, 1931
Schaller M. et al., 2015a, MNRAS, 451, 1247
Schaller M., Dalla Vecchia C., Schaye J., Bower R. G., Theuns T., Crain R. A., Furlong M., McCarthy I. G., 2015b, MNRAS, 454, 2277
Schawinski K. et al., 2014, MNRAS, 440, 889
Schaye J. et al., 2015, MNRAS, 446, 521
Shao S., Cautun M., Deason A. J., Frenk C. S., Theuns T., 2018, MNRAS, 479, 284
Shao S., Cautun M., Frenk C. S., 2019, MNRAS, 488, 1166
Simpson C. M., Grand R. J. J., Gómez F. A., Marinacci F., Pakmor R., Springel V., Campbell D. J. R., Frenk C. S., 2018, MNRAS, 478, 548
Springel V., 2005, MNRAS, 364, 1105
Tollerud E. J., Barton E. J., Bullock J. S., Trinh C., 2011, EAS Publications Ser., 48, 455
Tolstoy E., Hill V., Tosi M., 2009, ARA&A, 47, 371
Trayford J. W. et al., 2015, MNRAS, 452, 2879
Trayford J. W. et al., 2017, MNRAS, 470, 771
Turk M. J., Smith B. D., Oishi J. S., Skory S., Skillman S. W., Abel T., Norman M. L., 2010, ApJS, 192, 9
Wang J., Frenk C. S., Navarro J. F., Gao L., Sawala T., 2012, MNRAS, 424, 2715
Wetzel A. R., Hopkins P. F., Kim J.-h., Faucher-Giguère C.-A., Kereš D., Quataert E., 2016, ApJ, 827, L23
Zolotov A. et al., 2012, ApJ, 761, 71

This paper has been typeset from a TEX/LATEX file prepared by the author.